International Journal of Biological Macromolecules 193 (2021) 647–660

Contents lists available at ScienceDirect

International Journal of Biological Macromolecules

journal homepage: www.elsevier.com/locate/ijbiomac

Antisolvent *versus* ultrasonication: Bottom-up and top-down approaches to produce lignin nanoparticles (LNPs) with tailored properties

Camilla H.M. Camargos, Camila A. Rezende *

Physical Chemistry Department, Institute of Chemistry, University of Campinas–UNICAMP, P.O. Box 6154, Campinas, SP 13083-970, Brazil

ARTICLE INFO

Keywords:
Nanolignin
Lignin oxidation
Colloidal stability
Atomic force microscopy
DPPH scavenging
Diffuse reflectance spectroscopy

ABSTRACT

In spite of the increasing amount of literature on the production and application of lignin nanoparticles (LNPs), little or no attention has been paid so far to the influence of different production methods on the properties of these nanostructures. Herein, we propose a comprehensive study to assess the impact of several factors on the color, morphology, colloidal stability, antioxidant capacity, and UV-shielding performance of LNPs. LNPs were obtained by two different routes: a bottom-up approach based on the self-assembly in a solvent-antisolvent system with acetone/lignin/water; or a top-down approach based on the ultrasonication of never-dried lignin aqueous suspensions. The starting lignin was extracted from elephant grass leaves or stems, so that the influence of anatomical origin and molecular weight could also be investigated. Moreover, lignin was oxidized prior to being converted into LNPs, allowing for comparisons between different oxidation degrees. This study showed that interesting properties of LNPs can be easily tailored and combined focusing on the various applications of these versatile nanostructures. In a model application, different types of LNPs were incorporated into poly(vinyl alcohol)-based nanocomposites, modulating the UV-protection capability of the polymer matrix.

1. Introduction

Lignin is a primary by-product of papermaking [1] and bioethanol production [2], accounting for millions of tons of residues generated annually. Therefore, the preparation of lignin nanoparticles (LNPs) has emerged as a promising strategy to promote lignin valorization [3–5] and to enhance some of the valuable properties of this phenolic macromolecule, such as photo-protection, thermal stability, and antioxidant and antimicrobial capabilities [6,7]. Additionally, LNPs are dispersible in water and have a hydrophilic surface, allowing for their use in water-based systems and distinguishing them from most of native and technical lignins, which usually have a more hydrophobic character and limited solubility.

In grasses, softwoods, and hardwoods, the polymerization of monolignols (phenylpropanoid monomeric precursors of lignin) results in heterogeneous macromolecules containing different proportions of the structural units, namely *p*-hydroxyphenyl, guaiacyl, and syringyl. The composition of hardwood lignin is mainly based on guaiacyl units, while softwood lignin contains both guaiacyl and syringyl, and grass lignin contains guaiacyl, syringyl, and small concentration of *p*-hydroxyphenyl units [8]. Moreover, the complex three-dimensional structure of the recovered technical lignin also depends on the extraction procedure, which determines the fragmentation pathway, the changes in molecular weight, and the surface chemistry. For example, highly condensed kraft lignin or non-sulfur-containing lignins (alkaline, organosolv, and those from enzymatic hydrolysis) present different solubilities and physicochemical features [9]. These technical lignins are conventionally extracted during pulping or lignocellulosic biomass pretreatments and then isolated by precipitation, when the pH of lignin-enriched liquors is lowered by adding mineral acids [10,11]. After filtration and washing steps, the separated lignin can be converted into LNPs using either bottom-up or top-down approaches.

Bottom-up procedures comprise the self-assembly of solubilized lignin macromolecules [12–14] through a mechanism that is triggered by solvent exchange, as well as by antisolvent precipitation, also called solvent-antisolvent route [15]. In brief, the solvent-antisolvent method encompasses the addition of excess deionized water (antisolvent) to lignin dissolved in a water-miscible organic solvent [14], inducing the self-assembly driven by the hydrophobic effect. As an amphiphilic macromolecule, lignin segments interact either by hydrogen bonding, van der Waals forces, and π–π interactions [16]. These intermolecular forces also play a role for the aggregation of hydrophobic moieties in

* Corresponding author.
E-mail addresses: camilla.camargos@iqm.unicamp.br (C.H.M. Camargos), camilaiq@unicamp.br (C.A. Rezende).

https://doi.org/10.1016/j.ijbiomac.2021.10.094
Received 16 August 2021; Received in revised form 6 October 2021; Accepted 13 October 2021
Available online 23 October 2021

water, as well as for lignin self-assembling into spherical LNPs with ~100 nm average diameter [12]. This approach has been previously used to produce colloidally stable, highly antioxidant and UV-absorbing LNPs using alkaline lignin extracted from the leaves of elephant grass [6].

Top-down approaches, on the other hand, include the mechanical fragmentation or disintegration of macro/micro solid aggregates of bulk lignin into irregular-shaped LNPs or LNP aggregates [17–20]. These processes are usually carried out using aqueous suspensions of lignin. High shear homogenization yielded LNPs smaller than 100 nm after a 4-h mechanical treatment [19]. Probe-tip ultrasonication, *via* cavitation and strong collisions among aggregates, reduced lignin particles to sizes as small as 10–50 nm after a 60-min treatment [17]. Additionally, Agustin et al. [20] recently reported an energy-efficient and rapid method to produce LNPs smaller than 100 nm by 5-min ultrasonication of never-dried alkaline birch lignin.

Analogously to technical lignin, the size, shape, chemical properties, and stability of LNPs, particularly the self-assembled ones, are known to depend on lignin type, source, and extraction method, as well as on particle preparation routes [9]. However, a comprehensive study of multiple structure-property relationships has not been addressed so far and most of the published literature focus on the properties of LNPs produced by a single method using lignin extracted from one or different plants [3,4,17,19,21]. Few works explore variations in production conditions, such as the sonication time and water content of precursor lignin [20] or the control of lignin solution concentration [21,22] and antisolvent addition rate [16]. Moreover, there is still a lack of literature on the contribution of lignin surface chemistry for the enhancement of LNP features, which is highly valuable for the final applications of these nanostructures.

Functionalization of bulk lignin has been proven to impart different properties on LNP, such as reduced antioxidant activity and slightly greater UV-photoabsorbance in acetylated lignin [6], and higher cyto-compatibility in carboxylated lignin [23]. However, the impact of lignin oxidation prior to LNP production has not been reported so far. To the extent of our knowledge, only the oxidation of already formed LNPs has been studied. Mattinen and co-workers [24] performed a mild chemical oxidation with hydrogen peroxide and sonication at room temperature to promote LNP discoloration. Additionally, an enzymatic oxidation *via* laccase catalyzed cross-linking was performed to improve the LNP colloidal stability and reinforcement against dissolution in organic solvent (THF). The functionalization could increase LNP attractiveness as a biomaterial for applications in medicine, food, and cosmetic sectors [24,25]. In turn, functionalization prior to nanoparticle formation could ensure higher homogeneity to the internal and external structure of functionalized nanoparticles, in opposition to ulterior functionalization, when chemical substitutions are expected to prevail mainly on the accessible surface of the already formed LNPs. Oxidation using H_2O_2 as oxidizing agent has been proven to increase the amount of carboxylic functional groups, while reducing the amount of associated carbohydrates [26] and the antioxidant activity of alkaline lignin from sugarcane bagasse [27]. Likewise, He et al. [28] utilized a H_2O_2 protocol to obtain oxidized softwood kraft lignin with high content of carboxylate groups and outstanding performance as an anionic dispersant for clay suspensions.

Herein, we present an overview of the dependence of LNP properties on the production method, as well as on the anatomical origin and surface chemistry of lignin. For this purpose, elephant grass leaves and stems underwent a sequential acid-alkali pretreatment to separate lignin from the other components of the plant cell wall [29]. Lignin with high purity was extracted to the alkaline liquor and then isolated by a simple acidification method [6]. Subsequently, leaf and stem lignins, that is, macromolecules originated from a unique botanical source but two different anatomical parts, were oxidized using a mild $NaOH/H_2O_2$ pathway. Non-oxidized and oxidized pure lignins were converted into LNPs *via* solvent-antisolvent route (self-assembly) or by ultrasonication in never-dried aqueous systems. LNP dispersions presented different color features, and nanoparticle morphology, size, colloidal stability, and antioxidant activity were investigated. Moreover, the UV-shielding properties of all LNPs were evaluated after their incorporation into a poly(vinyl alcohol) matrix.

2. Experimental section

2.1. Materials

Feedstock: Elephant grass (*Pennisetum purpureum*) plants with *ca.* one year of growth were collected in the Institute of Animal Science (Instituto de Zootecnia - SP, Nova Odessa, Brazil). Plants were separated into leaves and stems, then oven dried at 60 °C for 24 h. Dry biomass was knife milled in a grinder equipped with a 10-mesh sieve.

Chemicals: Sulfuric acid (H_2SO_4, 98%), sodium hydroxide (NaOH, certified ACS), hydrogen peroxide (H_2O_2, 29%), acetone (P.A.), hydrochloric acid (HCl, 37%), sodium chloride (NaCl, certified ACS), potassium hydrogen phthalate (KHP, P.A.), acetic anhydride (Ac_2O, 97%), 1,4-dioxane (P.A.), and methanol (P.A.) were obtained from Synth (Diadema, Brazil). Alkali lignin with low sulfonate content (96%), acetyl bromide (99%), glacial acetic acid (99%), hydroxylamine-HCl (99%), 2,2-diphenyl-1-(2,4,6-trinitrophenyl)hydrazin-1-yl (DPPH radical), pyridine (99%), sodium dodecyl sulfate (SDS), and poly(vinyl alcohol) (PVA, 87–90% hydrolyzed) were purchased from Sigma-Aldrich (St. Louis, MO, USA). Tetrahydrofuran (THF, 99.9%, GPC grade) was supplied by PanReac AppliChem (Chicago, Illinois, USA).

2.2. Sequential acid-alkali pretreatment

Milled leaves and stems were sequentially treated with 1% (*v/v*) H_2SO_4 and 2% (*w/v*) NaOH, according to a method previously reported [30]. The first acid step was used to remove hemicellulose mainly, while the second alkali step was applied to extract the lignin fraction. Each step was carried out at 121 °C and 1.05 bar for 40 min in an autoclave. In addition to the pretreatment time, heating to working temperature took *ca.* 20 min and cooling to room temperature took *ca.* 40 min. 1:10 and 1:20 solid-to-liquid ratios (g of biomass mL^{-1} of solution) were used in first and second steps, respectively. Between steps and after the alkali step, the solid fraction was separated by filtration and abundantly rinsed with tap water. The alkaline liquors, containing *ca.* 20% of the total initial weight of raw leaves or 35% of the weight of raw stems, were recovered and used in the subsequent procedures.

2.3. Isolation of lignin

Alkaline liquors from leaves or stems were separately used in this step. These lignin-rich solutions with a concentration of *ca.* 1.2% (*w/v*) were acidified to pH 2 by dropwise addition of concentrated H_2SO_4 under constant magnetic stirring (400 rpm) [6]. Precipitation of large particles of bulk lignin was visually confirmed by the increased system turbidity. The precipitate was abundantly rinsed under vacuum filtering until the rinsing water reached pH 6–7. Part of the solid material recovered was oven dried at 40 °C for 12 h and another part was kept in aqueous suspension (never-dried fraction).

2.4. Oxidation of lignin

An adapted method using $NaOH/H_2O_2$ [28] was applied to oxidize leaf and stem lignins. 50 mL of 2% (*w/v*) NaOH were added to 50 mL of a never-dried aqueous suspension of 2% (*w/v*) lignin. The system was kept at 60 °C under constant magnetic stirring (400 rpm) for 10 min until the turbid suspension became a translucent solution. Then, 30 mL of 29% (*w/w*) H_2O_2 was added dropwise over 1 h to avoid excessive bubble formation. The reaction lasted for 2 h, then the solution was acidified (to reach pH 2) and the precipitated oxidized lignins were washed as

described in Section 2.3.

2.5. Production of lignin nanoparticles

Bottom-up approach: Adapting previously reported procedures [3,6,31], self-assembled lignin nanoparticles (SA-LNPs) and oxidized SA-LNPs (o-SA-LNPs) were prepared *via* a solvent-antisolvent route. Lignins or oxidized lignins were solubilized in a 9:1 (*v*/v) mixture of acetone/water at room temperature and under constant magnetic stirring (400 rpm) to form a 0.5% (*w/v*) lignin solution. Afterwards, the solution was quickly diluted with deionized water (1:100), resulting in aqueous dispersions of SA-LNPs or o-SA-LNPs.

Top-down approach: Adapting a previously reported method [17], ultrasonicated lignin nanoparticles (US-LNPs) and oxidized US-LNPs (o-US-LNPs) were prepared by sonicating never-dried suspensions of 0.1% (*w/v*) precipitated bulk lignin or oxidized lignin. The procedure was performed in a probe sonicator equipped with a 1 cm wide titanium macro-tip, operating at a 20 kHz frequency and 60% amplitude (330 W power output). Cavitation treatments were conducted for fixed suspension volumes (50 mL) in an ice bath for 15, 30, 60, and 90 min. The heating of the aqueous systems is highly detrimental to US-LNP production, as large visible fractal-like lignin clusters appear when the temperature rises. To evaluate the yields and morphology of such ultrasonicated systems in the presence of a surfactant, 0.2% (*w/v*) SDS was added to the lignin suspension prior to the sonication treatment.

After preparation, dispersions were vacuum filtered to remove larger aggregates and the yields of nanoparticle production were estimated in triplicate using an infrared balance for moisture determination. When required, concentrated aqueous dispersions were obtained by evaporation in an oven at 40 °C.

2.6. Preparation and evaluation of PVA/LNP composite films

An aqueous suspension of 1% (*w/v*) PVA was heated at 90 °C for 2 h under constant stirring (400 rpm). Then, LNP aqueous dispersions were incorporated into the cooled PVA solution to cast PVA films containing 10% (*w/w*) LNPs. The mixtures were oven dried at 40 °C for 12 h to produce films with a 2 mg cm^{-2} weight-to-area ratio and an average thickness of 109 ± 7 μm. Transmittance UV–Vis spectra of the films in the range of 200 to 800 nm, using a 0.5 nm resolution, were assessed by diffuse reflectance spectroscopy (DRS) in a UV-2450 spectrophotometer (Shimadzu, Kyoto, Japan).

2.7. Chemical characterization of bulk lignin

Compositional analysis of pretreatment liquors and of bulk lignins was carried out using high-performance liquid chromatography (HPLC, refractive index detector) and gravimetric methods according to standard protocols [32–34]. Acetyl bromide soluble lignin (ABSL) was quantified using an indirect colorimetric method based on the dissolution of bulk lignins in acetyl bromide (acid medium) [29]. UV–Vis absorption spectra of non-oxidized and oxidized bulk lignins were collected in a Varian's Cary® 50 UV–Vis spectrophotometer (Agilent Technologies, Santa Clara, USA) using 1 cm pathlength quartz cuvettes. Calibration curves were obtained by acquiring the absorption spectra of alkaline solutions (2 mol L^{-1} NaOH) containing lignins or oxidized lignins at concentrations from 5 to 80 mg L^{-1}. For comparison, a commercial alkali lignin with low sulfonate content was also analyzed. Extinction coefficient was calculated using the Beer-Lambert law. ATR-FTIR spectra of non-oxidized and oxidized lignins were obtained in an Agilent Cary® 630 FTIR spectrometer with ATR sampling module using a spectral resolution of 4 cm^{-1} and 128 scans. Gel permeation chromatography (GPC) of acetylated lignin in THF (3 mg mL^{-1}) was conducted using a Waters 1525 Binary HPLC Pump (Milford, USA) with a refractive index detector. Prior to GPC analysis, lignin was acetylated adapting a previous protocol [35], in which lignin powders (oxidized and non-oxidized) reacted with 1:1 (*v/v*) pyridine/acetic anhydride, in the dark, under constant magnetic stirring (400 rpm) at room temperature for 120 h. The reaction was quenched, and the acetylated lignin was re-precipitated by adding cold deionized water (pH 2 adjusted with HCl). Results were reported as number-average molecular weight (M_n), weight-average molecular weight (M_w), and dispersity (Đ).

2.8. Morphological characterization of bulk lignin and LNPs

Optical microscopy (OM) images of bulk lignin (dried powder and never-dried suspension) were obtained in a Nikon Eclipse E800 microscope coupled with a Nikon DS-Ri1 camera (Tokyo, Japan), using bright field mode with 4×, 10×, 20×, and 40× magnification lens. SEM micrographs of bulk lignin and LNPs were acquired at 5 kV, using secondary electron detector in a Quanta FEG 250 microscope (FEI, Hillsboro, USA). SEM sample preparation included Ir sputter coating with a 11.3 mA current for 120 s in a BAL-TEC MED 020 sputter coater (Balzers, Liechtenstein). SEM images were analyzed using ImageJ software (imagej.nih.gov/ij/). AFM height, phase, and amplitude images of LNPs were obtained in a Shimadzu SPM 9600 microscope using non-contact mode and a NCHR probe (curvature radius: 8 nm). For both AFM and SEM sample preparation, 10 μL of LNP dispersions (5–10 μg mL^{-1}) were deposited on mica substrates and then dried for at least 4 h at room temperature before analysis. More than five AFM images were captured per sample with a scanning rate of 1 Hz (1 line s^{-1}) and a 512-pixel resolution. Images were treated (row leveling and false color scale adjustment) and analyzed in Gwyddion 2.56 (Gwyddion.net). In AFM analysis, diameters were estimated as the height (z) for individualized spherical nanoparticles (SA-LNPs) and as the lateral (largest) width for irregularly shaped globular aggregates (US-LNPs). In both SEM and AFM, at least 130 LNPs were measured to build size distribution histograms.

2.9. Surface charge and colloidal stability of LNPs

Conductometric titration was performed in a Starter 3100M pH & conductivity bench meter (OHAUS, Parsippany, USA) to quantify the amount of ionizable functional groups (weak acids) onto lignin and LNP surface. Adapting previously reported methods applied for cellulose titration [30,36], 2.5 mL of 0.05 mol L^{-1} HCl were added to 50 mL of 0.01–0.1% (*w/v*) lignin suspension or 0.01–0.1% (*w/w*) LNP dispersion. Then, the system was titrated with a standardized 0.01 mol L^{-1} NaOH solution. The content of ionizable groups, measured in mmol g^{-1}, was estimated considering the NaOH volume added while the conductivity was constant. DLS and zeta potential measurements were performed in a Malvern Zetasizer® Nano ZS-Zen 3600 (Malvern, UK) using a standard DTS1070 disposable folded capillary cell to assess the stability of LNPs in aqueous dispersions over pH 2–12. Mean hydrodynamic diameters were reported as number-weighted diameter for SA-LNPs (spherical shape) and intensity-averaged diameter for US-LNPs (irregular shape). 1 mol L^{-1} NaOH or HCl were used for pH adjustments of different aliquots of LNPs. All measurements of mean hydrodynamic diameter and zeta potential were performed with a fixed 173° scattering angle, in triplicates of at least 11 scans each.

2.10. Antioxidant activity of bulk lignin and LNPs

Adapting a previously reported procedure [6,37,38], the antioxidant activity of lignin in solution and LNPs in dispersion was determined in terms of DPPH radical scavenging activity *via* a colorimetric assay. In brief, 2 mL of 65 μmol L^{-1} DPPH• in methanol were added to 1 mL of 0.15 mg mL^{-1} lignin in 90% (*v/v*) dioxane or 1 mL of 0.15 mg mL^{-1} LNP aqueous dispersion. DPPH• concentration immediately after adding it to lignin solution or LNP dispersion (0 min) and after 16 and 30 min was examined, away from direct light, using the relative intensity of the absorption band at 515 nm (λ_{max}) measured by UV–Vis spectroscopy.

Blanks were prepared by adding 2 mL of DPPH• solution to 1 mL of 90% (*v/v*) dioxane or 1 mL of deionized water, respectively, for the assessment of the antioxidant capacity of lignin in solution and LNPs in dispersion. All measurements were carried out at room temperature, in duplicates. The DPPH• scavenging activity was calculated according to eq. 1:

$$\%\text{Scavenging} = \frac{(Abs\ blank) - (Abs\ sample)}{Abs\ blank} \times 100 \quad (1)$$

where *Abs blank* refers to the relative absorbance at 515 nm of the systems containing only solubilized DPPH• after 0, 16, and 30 min, while *Abs sample* is the absorbance of each sample at the same specific time.

3. Results and discussion

3.1. Properties of lignins extracted from biomass leaves and stems

A sequential acid-alkali treatment was initially performed to extract pure lignin for nanoparticle preparation [6], as depicted in Fig. 1. During the first acid step, most of the hemicellulose contained in elephant grass leaves and stems was removed [29,30]. Afterwards, most of the lignin, which corresponded to approximately 20–30% (*w/w*) of the raw biomass, was solubilized in the alkali step and extracted to the liquid fraction. Then, the alkaline liquors were treated to isolate lignin.

Klason lignins, that is, the acid insoluble lignin fractions, were recovered by medium acidification with a few drops of concentrated sulfuric acid. Up to 69% of the total amount of lignin contained in the alkaline liquor was precipitated as lignin aggregates with dimensions of hundreds of micrometers (Fig. S1). This extraction yielded an amount corresponding to 42% and 44% of the initial content of lignin in raw leaves and stems, respectively. Similar extraction yields were previously reported for lignin isolated from elephant grass leaves [6].

Lignin isolated from leaves or stems presented typical brownish coloration (Fig. 2A,C), though with different shades. Lignin brown color is related to the condensed chemical structure of the macromolecule and the presence of chromophores that promote high absorption capability in the ultraviolet/visible region [1,39,40]. The conjugated π-bonds contribute to a greater absorption at near-ultraviolet and blue wavelengths, resulting in an overall orange-to-brown color [41,42].

UV–Vis spectra showed the characteristic profile of the macromolecule in alkaline solution, with a maximum absorbance at around 285 nm for stem lignin, and 288 nm for leaf and commercial lignins (Fig. S2). This characteristic band could be assigned to sinapyl, coniferyl, and coumaryl alcohols, the monolignols that participate in lignin biosynthesis [43]. The relative intensity of this band was linearly dependent on lignin concentration ($R^2 \geq 0.99$).

The high purity of lignin was estimated as 95.0 ± 0.4% using UV–Vis calibration curves. Compositional analysis also indicated statistically equivalent content of acid insoluble lignin, 94.4 ± 0.2%. The method of ABSL, in turn, resulted in total concentrations of 98 ± 1% and 99 ± 1% for lignin from leaves and stems, respectively. The last method can provide overestimated results due to the simultaneous oxidative

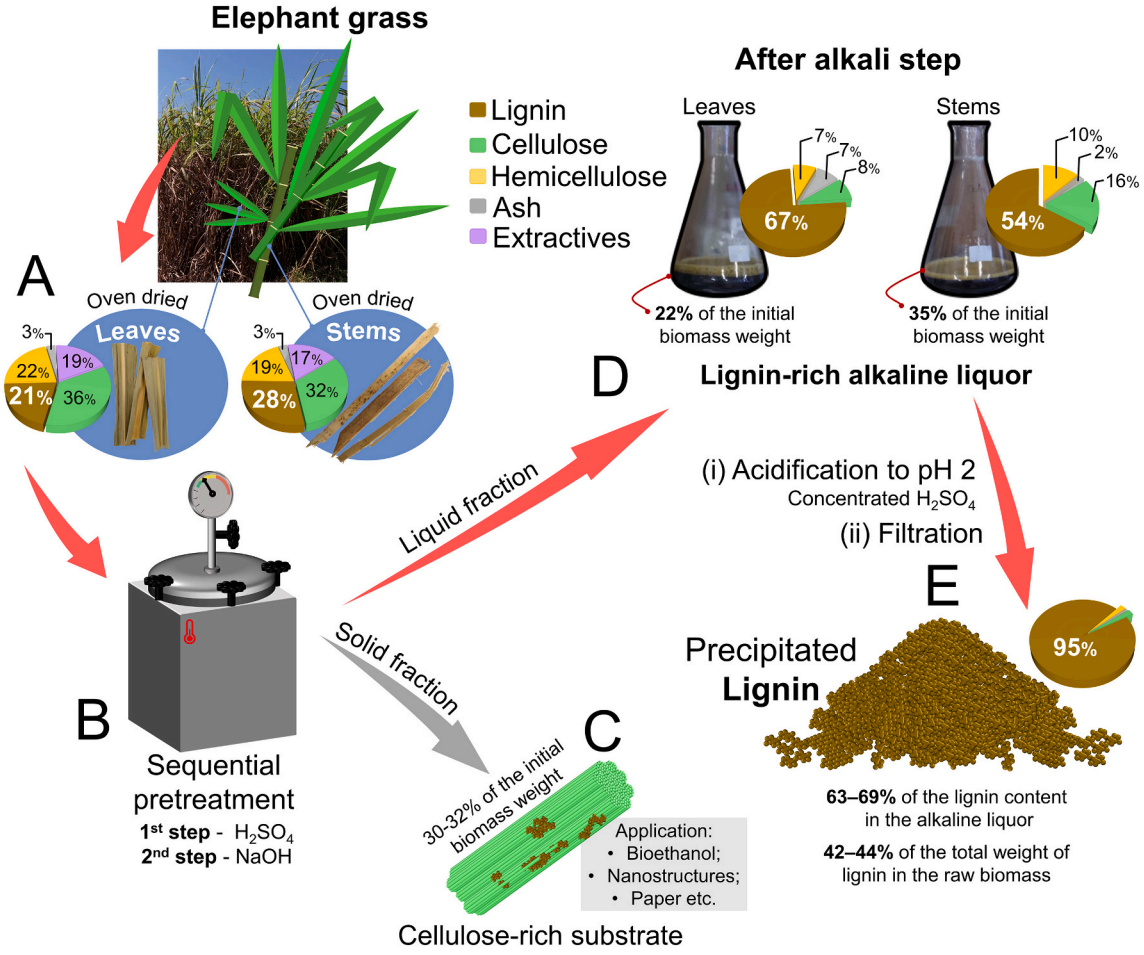

Fig. 1. Depiction of the fractionation of (A) raw elephant grass leaves and stems, respectively, containing 21% and 28% (*w/w*) of lignin. (B) A sequential acid-alkali pretreatment with 1% (*w/v*) H_2SO_4 and then 2% (*w/v*) NaOH was carried out to separate (C) a solid cellulose-rich substrate that could be used for several purposes [30], and (D) a lignin-rich alkaline liquor. This liquid fraction was (i) acidified to pH 2 by dropwise addition of concentrated sulfuric acid and subsequently (ii) washed and filtered to isolate (E) 95% pure precipitated lignin.

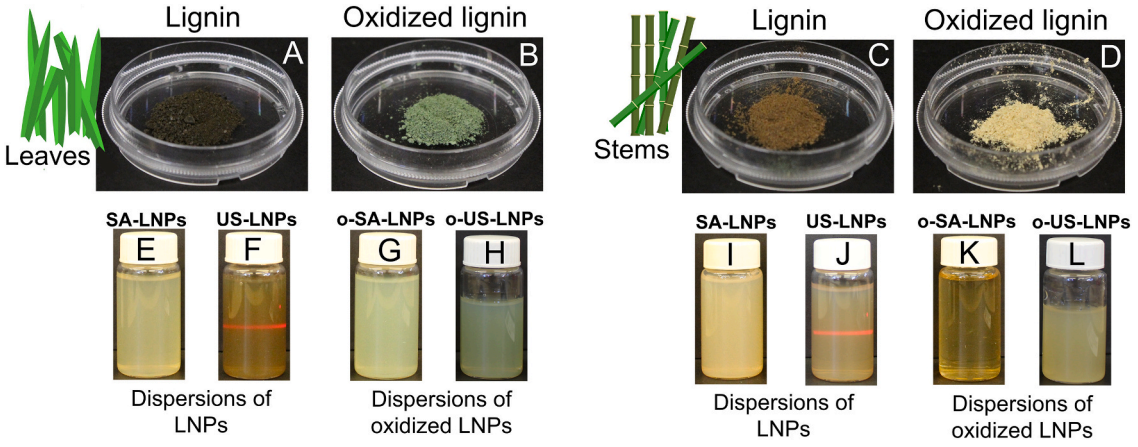

Fig. 2. Photographs under visible light of (A) non-oxidized and (B) oxidized leaf lignin, (C) non-oxidized and (D) oxidized stem lignin, as well as of (E–L) aqueous dispersions of non-oxidized and oxidized LNPs. Red laser scattering in (F, J) demonstrates the Tyndall effect present in all LNP dispersions. (For interpretation of the references to color in this figure legend, the reader is referred to the web version of this article.)

degradation of structural carbohydrates during sample acid incubation [44]. It is clear, however, that the lignin purity is quite high, independently of the determination method.

After isolation, lignins underwent mild oxidation with diluted $NaOH/H_2O_2$ solution. Oxidized lignin presented different coloration when compared to the brownish non-oxidized lignins. Leaf oxidized lignin was greenish (Fig. 2B), while the stem oxidized one was yellowish (Fig. 2D). ATR-FTIR confirmed changes in the lignin chemical structure after oxidation (Fig. 3A, B). A new absorption band at 1715 cm^{-1} was assigned to C═O stretching vibrations in oxidized lignin [45]. Additionally, the relative intensity of the absorption band at 2845 cm^{-1} increased. This band was related to the asymmetric C—H stretching in methyl and methylene groups of lignin side chains [46,47]. Therefore, there was likely a proportional growth in the amount of lignin end- and side-chain groups, indicating further fragmentation during oxidation process. GPC analysis (Fig. 3C) corroborated this assumption, as the weight-average molecular weight (M_w) decreased from 7000–8000 g mol^{-1} in non-oxidized bulk lignins to around 5000 g mol^{-1} in oxidized lignins. Such reduction in the molecular weight was accompanied by a decline in molar mass dispersity, which became much narrower (1.4 in non-oxidized to 1.1 in oxidized lignin), as shown in Table S1. Similarly, oxidation using H_2O_2 imparted a reduction in the M_w from 16,770 g mol^{-1} in softwood kraft lignin to 14,825 g mol^{-1} in its oxidized counterpart [28].

Moreover, ATR-FTIR (Fig. 3A, B) also showed that the cleavage of covalent bonds between phenylpropane units did not disrupt the aromatic structure of lignin, as confirmed by the preservation of absorption bands at 2920 cm^{-1}, 1503 cm^{-1}, and 1116 cm^{-1}. The first band was assigned to C—H stretching in aromatic methoxy groups, the second to C═C stretching in aromatic ring [48], and the last to aromatic C—H in-plane deformation [47]. Although the relative intensity was lower, UV–Vis spectra of oxidized lignins also showed the characteristic absorption band of lignin at about 280 nm (Fig. S3). Absorption (extinction) coefficients decreased from 22.54 ± 0.78 L g^{-1} cm^{-1} in the non-oxidized to 17.35 ± 0.76 L g^{-1} cm^{-1} in the oxidized leaf lignin, while for the stem lignin the reduction was from 25.84 ± 0.98 to 14.13 ± 0.20 L g^{-1} cm^{-1} after oxidation.

3.2. Bottom-up and top-down approaches to produce lignin nanoparticles

Two different approaches were used to convert non-oxidized and oxidized lignin from leaves and stems into LNPs (Fig. 4). The bottom-up method depicted in Fig. 4A consisted of adding water as an antisolvent to acetone solutions of lignin. The hydrophobic effect and the π–π interactions between the hydrophobic moieties of the macromolecule in water were the driving forces for the self-assembly of lignin into nanoparticles [12,16]. Self-assembled LNPs (SA-LNPs) were recovered with a 93 ± 4% yield. Equivalent results were previously achieved for elephant grass leaves (93 ± 3%) [6] and corn biomass (93 ± 6%) [3].

In the top-down method (Fig. 4B), on the other hand, aqueous suspensions of never-dried bulk lignin were mechanically treated using probe-ultrasonication, that is, liquid cavitation promoted the further disintegration of solid lignin aggregates into individual nanoparticles or LNP aggregates [17]. The recovery ratios of US-LNPs increased as the ultrasonic treatment lasted longer. Sonication for 15 min, 30 min, and 60 min resulted in yields of 18 ± 4%, 45 ± 3%, and 85 ± 3%, respectively. Increasing the sonication time to 90 min led to a 90 ± 2% yield. Considering the greater energy consumption and modest improvement

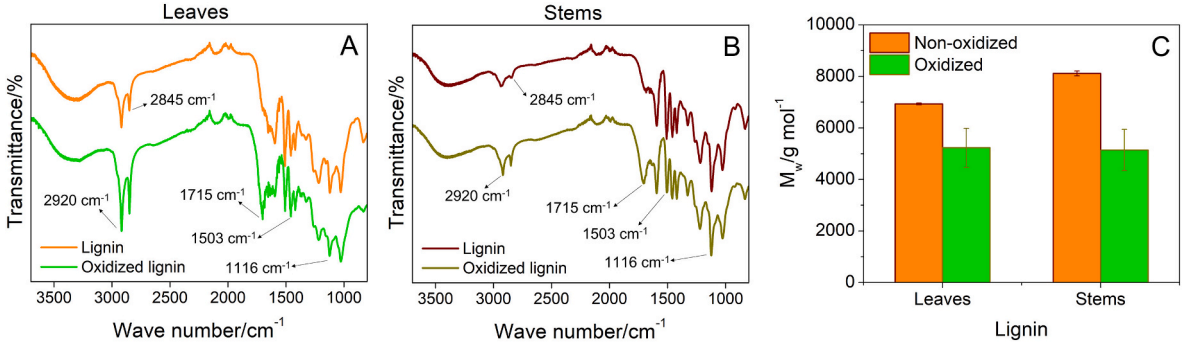

Fig. 3. ATR-FTIR spectra of non-oxidized and oxidized lignins extracted from (A) leaves and (B) stems. (C) Molecular weight (M_w) measured by GPC of non-oxidized and oxidized lignins from leaves and stems. Results expressed as the average and standard deviation of duplicates.

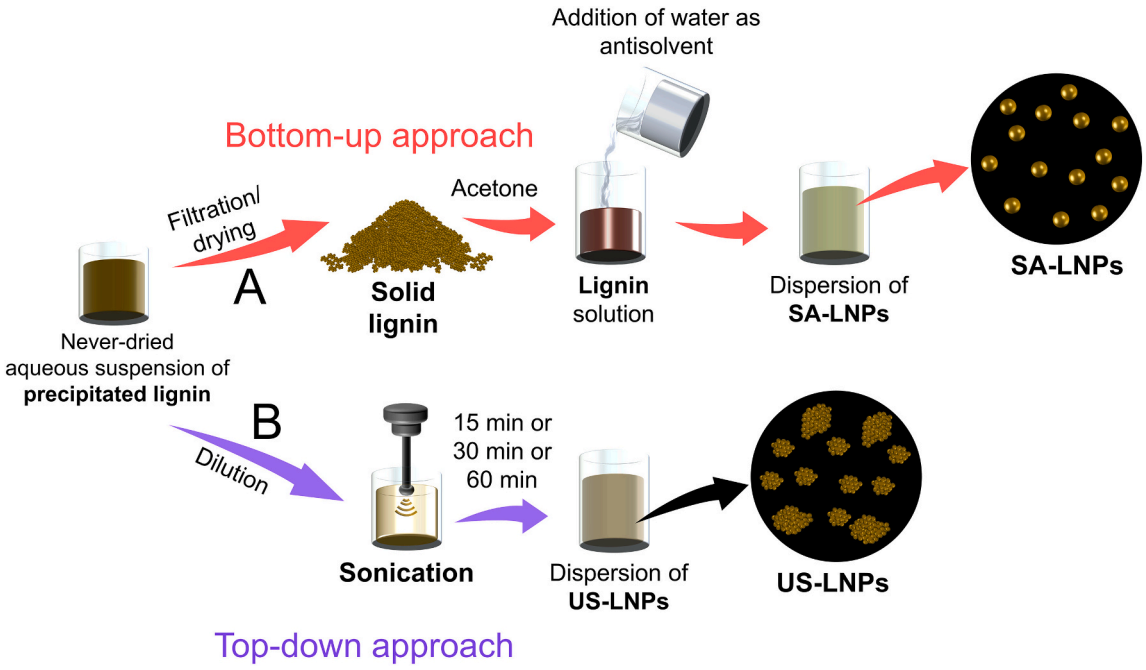

Fig. 4. After lignin isolation, two methodologies were applied to produce LNPs. (A) In the bottom-up approach, the aqueous suspension of precipitated lignin was filtered and dried, yielding a solid lignin powder which was solubilized in acetone. Then, excess deionized water was added to the lignin solution, resulting in an aqueous dispersion of self-assembled nanoparticles (SA-LNPs). (B) In the top-down approach, the never-dried lignin suspension was diluted with deionized water and then underwent probe-sonication for 15 min, 30 min, or 60 min, yielding ultrasonicated nanoparticles (US-LNPs) also in aqueous dispersion.

in the conversion rate, this longer procedure was not further investigated.

Different plant anatomical origins and production methods, as well as oxidation degrees imparted different visual aspects to the LNP dispersions. Aqueous dispersions of SA-LNPs present similar light yellowish color (Fig. 2E, I), while US-LNPs are brownish (Fig. 2F, J). Moreover, dispersions of o-SA-LNPs and o-US-LNPs present lighter color than their non-oxidized analogues. Oxidized LNPs derived from leaf lignin are more greenish (Fig. 2G, H), while those derived from stem lignin are more yellowish (Fig. 2K, L). All dispersions showed Tyndall effect, that is, a laser beam underwent light scattering when passing through these colloidal systems (Fig. 2F, J). The color of lignin and LNPs is not a topic frequently discussed in literature, but it can have important consequences for end applications, for instance in coatings and cosmetics. As demonstrated here, material coloration is highly dependent on the anatomical source and oxidation degree of starting lignin.

3.3. Morphological properties of self-assembled lignin and oxidized lignin nanoparticles

As shown in Fig. 5 and Fig. S4, SA-LNPs and o-SA-LNPs presented characteristic spherical morphology [14,16,49], and prior oxidation of lignin did not prevent the macromolecules from self-assembling into nanospheres. SEM images (Fig. 5A, D) evidenced the presence of single holes on the surface of some nanospheres. This feature was also observed in previous studies [6,16] and is probably an effect of solvent evaporation under high vacuum and temperatures during SEM sample preparation and analysis. Xiong et al. [16] suggested that the solvent trapped inside the nanoparticle core breaks through the LNP surface at higher temperatures and forms these holes. In fact, such morphological characteristics were absent in AFM images, in which both sample preparation and image acquisition are performed under environmental conditions.

All self-assembled LNPs presented skewed diameter distribution (Fig. 5G–L). For leaf and stem SA-LNPs, the average diameters determined by SEM and AFM slightly diverged, as expected, since the size was measured as Ir-coated particle width in SEM and particle height in AFM. While the diameters of SA-LNPs from leaves and stems were very similar, those of o-SA-LNPs were significantly smaller. Average diameter halved from *ca.* 50 nm in non-oxidized to *ca.* 25 nm in oxidized SA-LNPs. This difference was likely due to lignin cleavage after oxidation, which resulted in smaller macromolecular soluble moieties/fragments (M_w up to 3000 g mol^{-1} smaller), which could self-assemble into smaller nanospheres. Specifically for spruce lignin samples with relatively high molecular weight, Pylypchuk et al. [22] reported a similar trend of increasing size of SA-LNPs as the M_w increased. Lignin fractions with M_w of 3080 g mol^{-1} formed SA-LNPs with an average size of 80 nm, while fractions with M_w of 6360 g mol^{-1} formed SA-LNPs with an average size of about 100 nm. The observed trend was opposite for lignins with lower molecular weight, and the authors argued that macromolecular fragments with very small M_w (~1000 g mol^{-1}) present greater content of phenolic hydroxyl groups, which favored the growth of larger nanoparticles. Here, in addition to the decrease in M_w and dispersity, lignin oxidation conferred a charge effect by introducing carboxylic acid groups, which resulted in the production of o-SA-LNPs smaller than the corresponding SA-LNPs.

3.4. Morphological properties of ultrasonicated lignin and oxidized lignin nanoparticles

US-LNPs and o-US-LNPs were produced with fixed ultrasound power and variable treatment time. These nanoparticles or fragmented aggregates presented flattened, irregular/globular-like shape (Fig. 6, Fig. 7, and Figs. S5–S7), with some exhibiting *quasi* spherical morphology (especially the oxidized US-LNPs obtained after 60-min sonication), as shown by AFM topography, amplitude, and phase images (Fig. S5D and Fig. S6C, D). Herein, the AFM topographical height was smaller than the lateral width for most of the particles or clusters observed, so the latter dimension was taken as the US-LNP diameter. Likewise, SEM micrographs revealed the detachment of lignin plates from larger lignin fragments after 15 min of sonication (Fig. S8).

Optical micrographs demonstrated that flat and layered micrometric

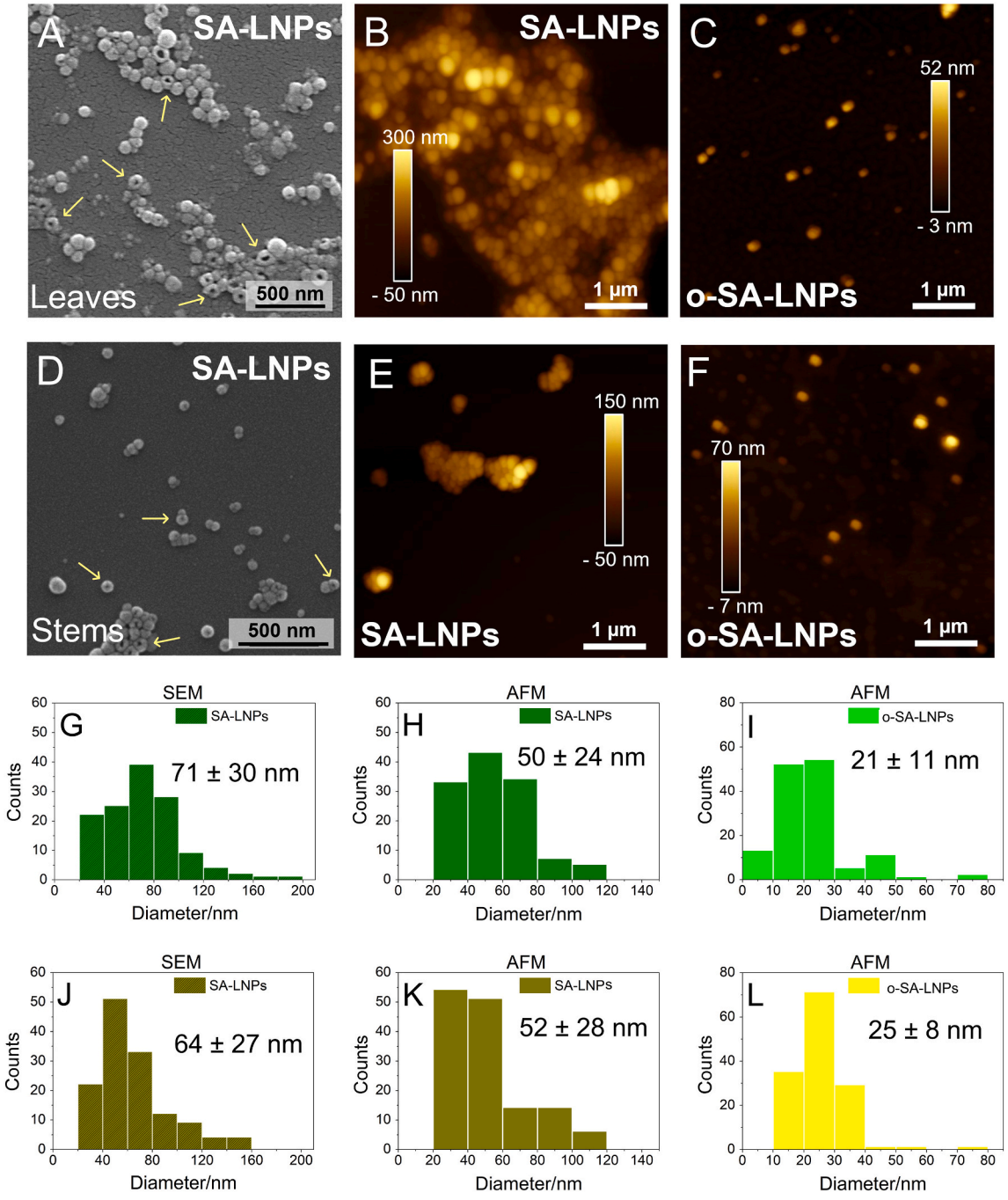

Fig. 5. Images obtained by (A, D) SEM and (B, C, E, F) AFM (topography) of SA-LNPs and o-SA-LNPs from leaves and stems. Corresponding histograms of diameter size distribution for (G–I) leaf and (J–L) stem SA-LNPs and o-SA-LNPs. Yellow arrows in (A, D) highlight nanospheres with holes. Particle diameter was measured as the lateral dimension (width) in SEM and the height (z) in AFM topography images. (For interpretation of the references to color in this figure legend, the reader is referred to the web version of this article.)

particles with a shale-like morphology were already present in never-dried suspensions of untreated lignins, thus indicating that lignin plates were formed during lignin precipitation from the alkaline liquor (Fig. S9). Such observation suggested that cavitation and aggregate-aggregate collisions initiated the size reduction probably *via* a mechanism of mechanical exfoliation, generating irregularly shaped particles. Previous works [17,18] also found LNPs produced by ultrasonication to be irregular in shape.

As shown in AFM phase images, the morphology of US-LNPs was very distinct from that of SA-LNPs (Fig. 7G, H). While self-assembled LNPs typically showed spherical morphology, with smooth surface (Fig. 5), ultrasonicated LNPs were flat, granular, and heterogeneous in shape, being composed of a bunch of small *quasi* spherical entities (Fig. 6F, Fig. 7F, and Figs. S5, S6) likely formed during the isolation of bulk lignin. In fact, the acidification of alkaline liquors promotes protonation of hydroxyl and carboxylic acid functional groups of lignin, leading to the overall precipitation of the macromolecules into random aggregate-like, granular/globular structures [50]. Although at different scales, such globular morphology visualized as micrometric conformations in the precipitated lignins (Fig. S9) seems to have been transposed to some extent to the nanometer scale in the US-LNPs (Figs. 6 and 7).

Sonication for 15 min was enough to reduce the dimension of lignin

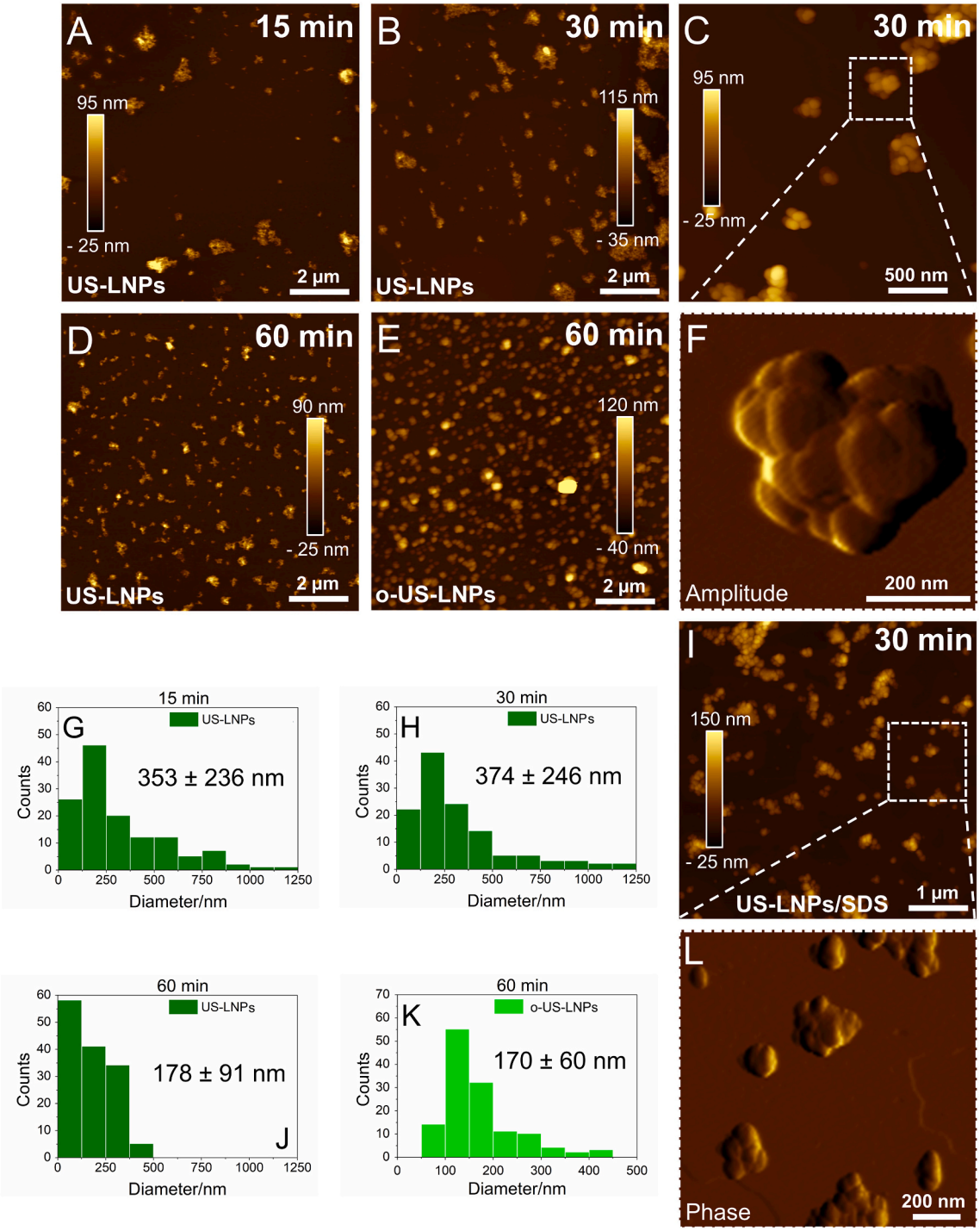

Fig. 6. AFM (A–E, I) topography, (F) amplitude, and (L) phase images of US-LNPs and o-US-LNPs from leaves. Images (F) and (L) magnify a detail of (C) and (I), respectively. Corresponding histograms of diameter size distribution for US-LNPs obtained by sonication during (G) 15 min, (H) 30 min, and (J) 60 min, as well as for (K) o-US-LNPs sonicated for 60 min. As nanoparticles were flat, the diameter was measured as the lateral dimension (larger width) in AFM topography images (tip radius of curvature: 8 nm).

aggregates to the nanoscale (Figs. 6A, G and 7A, I). As the sonication time increased, the average diameter decreased, and the shape of the nanoparticles became more homogeneous, especially for stem US-LNPs (Fig. 7C and Fig. S6C, D). However, average diameter and skewed size distribution for ultrasonicated samples only significantly changed when ultrasonication time raise to 60 min (Figs. 6D, E, J, K and 7C, D, K, L). Then, the nanoscale agglomerates of US-LNPs and o-US-LNPs were *quasi* spherical-like domains with significantly smaller diameters and narrower size distributions, probably due to leveling-off and exhaustive breakdown of lignin fragments. In fact, the size of the globules or small entities forming the US-LNPs was quite constant, while the size of formed nanostructures (the US-LNPs themselves) was dependent on the sonication time. Similar reduction of interparticle aggregation owing to increasing ultrasonication time was reported before [18], but a thorough AFM analysis of these morphological features was still lacking.

The behavior and resulting features of sonicated systems in the presence of a surfactant were also investigated as an attempt to ascertain whether the globular aggregates (US-LNPs) originate in the sonication

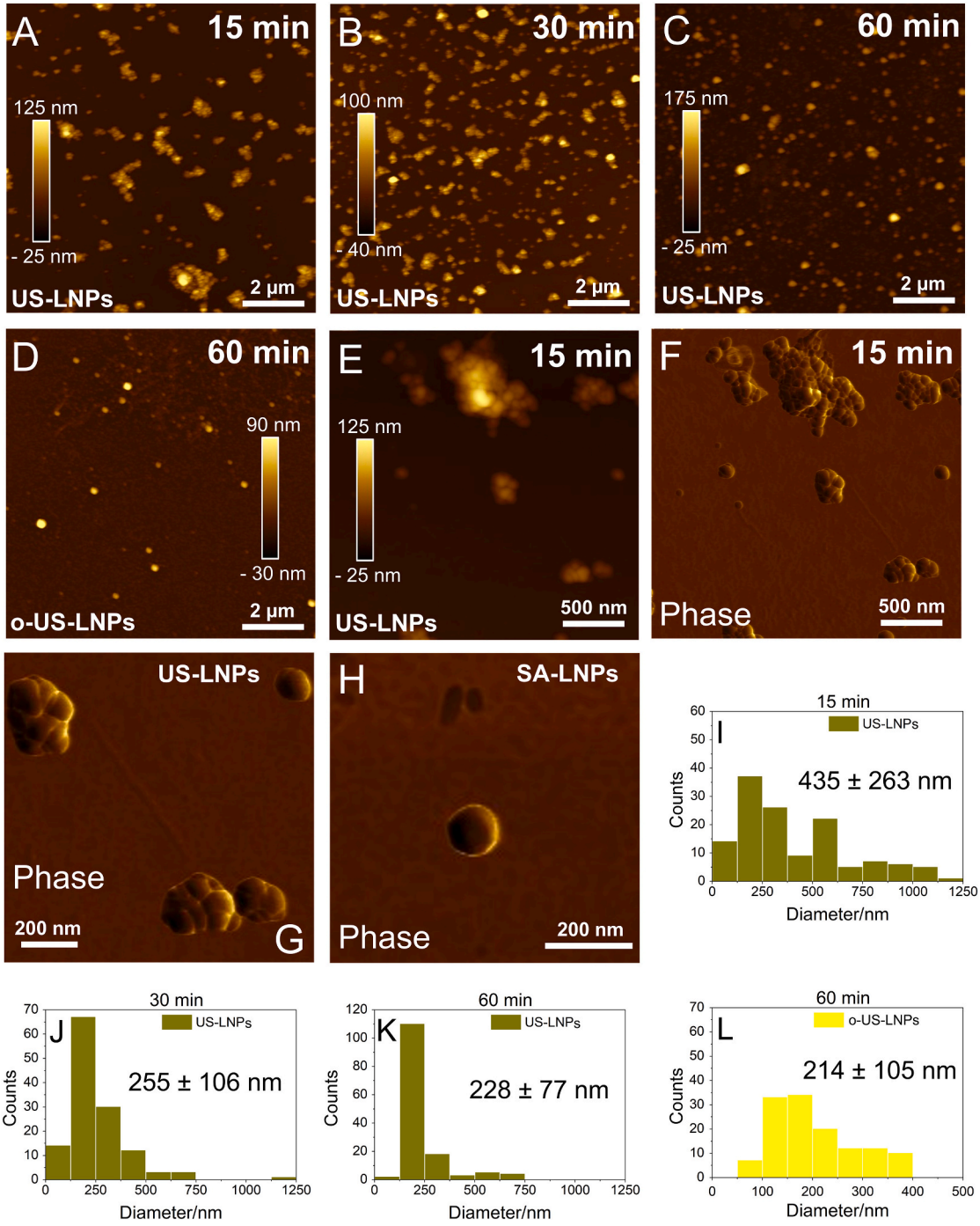

Fig. 7. AFM (A–E) topography and (F, G) phase images of US-LNPs and o-US-LNPs from stems. Images (G) and (H) are representative phase images of US-LNPs (15 min) and a SA-LNP, respectively. Corresponding histograms of diameter size distribution for stem US-LNPs obtained by sonication during (I) 15 min, (J) 30 min, and (K) 60 min, as well as for (L) o-US-LNPs sonicated for 60 min. As ultrasonicated nanoparticles were flat, the diameter was measured as the lateral dimension (width) in AFM topography images (tip radius of curvature: 8 nm).

process or if individualized nanometric globules are formed in sonication and then aggregate later, during the drying process prior to microscopy analysis. Being aware that lignin in aqueous suspension presents a very negative zeta potential, sodium dodecyl sulfate (SDS, anionic surfactant) was added to increase dispersion and prevent – through electrostatic and steric mechanisms – the formation of aggregates/flocs during the preparation and analysis of nanoparticles.

In the presence of SDS, the conversion yields of lignin into US-LNPs were 71 ± 3%, 79 ± 3%, 85 ± 1%, and 91 ± 2%, respectively, under sonication for 15, 30, 60, and 90 min. This result suggests that at times shorter than 30 min the surfactant favored to some extent the separation of aggregates into smaller particles and/or prevented such particles from flocculating. At times longer than 30 min, the presence of the surfactant did not significantly influence the yields, which were levelled-off compared to the systems without SDS. The overall morphology did not change significantly (Fig. 6I, L and Fig. S7), except for the average diameters, which were smaller (up to 148 nm) in the presence of SDS than in its absence (up to 180 nm). The presence of large aggregates of nanoparticles was observed in both cases, thus evidencing that US-LNP morphology was mainly determined by the sonication step and was not

merely an effect of the drying process.

Furthermore, contrasting the results for self-assembled nanoparticles, prior oxidation of lignin caused no difference between the average diameter of US-LNPs and o-US-LNPs. In self-assembly, the mechanisms of ordering and nanosphere formation depend on the size (M_w) and surface chemistry of the macromolecular fragments of lignin that will yield SA-LNPs and o-SA-LNPs, so the latter were smaller than the former. In the case of ultrasonication, the aggregates formed during lignin precipitation are simply mechanically fragmented afterwards. Therefore, the results of this process depend more on the ultrasonic treatment and the conformation of the aggregates themselves than on factors such as macromolecule size and surface chemistry. Consequently, the top-down approach (ultrasonication) yielded larger particles than the bottom-up method (antisolvent).

3.5. Colloidal stability of lignin and oxidized lignin nanoparticles

Conductometric titration of weak acids indicated that increasing both the surface area and the oxidation degree contributed to the higher amount of ionizable groups (IG) on the surface of LNPs. The effect of surface area was evidenced by the increased IG content in all LNPs (oxidized or not) compared to their respective bulk precursor lignins in water (Fig. 8A). The effect of oxidation, in turn, was demonstrated by the much higher IG content in the oxidized lignins (2.3 ± 0.1 mmol g^{-1} of leaf lignin and 3.0 ± 0.3 mmol g^{-1} of stem lignin) than in the bulk lignins before oxidation (0.21 ± 0.05 mmol g^{-1} and 0.16 ± 0.04 mmol g^{-1}). In agreement, o-SA-LNPs had the highest amount of ionizable groups among the samples due to the combination of both surface area and oxidation effects. The predominant presence of hydrophilic groups (phenolic hydroxyl and carboxylic acid functional groups) on the surface of self-assembled and oxidized particles was thus a consequence of their preparation method. The self-assembly process allows the bending of flexible lignin fragments in order to favor interactions among the hydrophobic moieties into the inner core of the nanoparticles, while their hydrophilic groups are directed towards the outer shell [6,14].

In the case of US-LNPs, the cavitation procedure increased the local

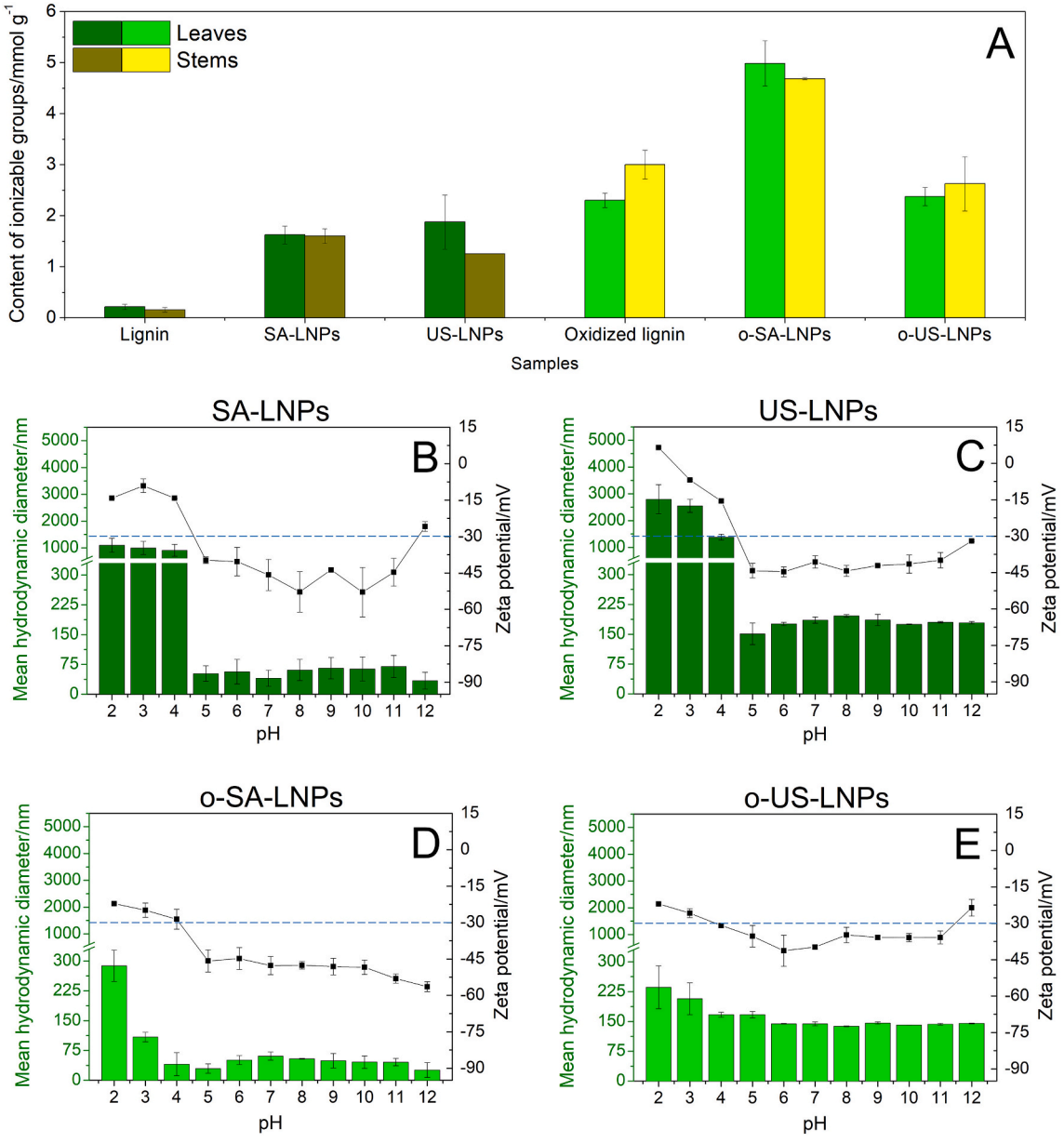

Fig. 8. (A) Content of ionizable groups on the surface of lignins and LNPs. (B–E) Mean hydrodynamic diameter (left axis) and zeta potential (right axis) as a function of pH for samples of non-oxidized and oxidized LNPs from leaves. Dotted lines indicate the – 30 mV limit in the ζ potential axis.

system temperature and pressure, generating radical species of hydroxyl groups in aqueous media in the presence of air [17]. Agustin et al. [20] suggested that ultrasonication can induce changes in the surface charge of LNPs by exposing surface carboxyl or phenolic groups. Additionally, the ultrasonic treatment can cause the homolytic cleavage of β–O–4 alkyl phenyl ether bonds, producing reactive species onto the nanoparticle surface [51]. Hence, ultrasonication also enhanced the content of ionizable groups in US-LNPs but did not contribute significantly for o-US-LNPs, as oxidized lignin possessed already a great content of weak acids on the surface.

As confirmed by zeta potential and DLS measurements, all LNPs presented improved colloidal stability (Fig. 8B–E and Fig. S10). Zeta potentials more negative than – 30 mV [52] indicate that the nanoparticles were stabilized in water through electrical double layer repulsion [53] in a broad pH range. This mechanism was sensitive to the pH of the aqueous media and generally prevailed only above pH 3 due to the protonation of lignin phenolic and carboxylic groups at low pH [54]. Herein, the stabilization in terms of particle surface charge and mean hydrodynamic diameter extended over pH 5 to 11 for non-oxidized LNPs from both leaves and stems (Fig. 8B, C and Fig. S10A, B). Similar behavior was previously reported for self-assembled LNPs produced from elephant grass [6] and corn biomass [3,55]. Additionally, oxidized LNPs, which presented higher content of ionizable groups on the surface, showed colloidal stability in a broader range from pH 4 to 12 (Fig. 8D and Fig. S10C) and pH 3–4 to 11 (Fig. 8E and Fig. S10D), respectively for o-SA-LNPs and o-US-LNPs. Also, outside the pH range of satisfactory colloidal stability, the mean hydrodynamic diameters of oxidized LNPs were always smaller than those of the non-oxidized LNPs, probably due to a longer lasting charge effect (greater content of anionic groups in o-SA-LNPs and o-US-LNPs).

3.6. Antioxidant activity of lignin and oxidized lignin nanoparticles

The antioxidant activity of leaf and stem lignins in solution, their oxidized counterparts, and self-assembled or ultrasonicated LNPs was assessed using the DPPH radical scavenging assay. At fixed concentration (50 μg mL^{-1}), SA-LNPs and US-LNPs scavenged up to 56% of the initial amount of DPPH• immediately at the beginning of the experiment (Fig. 9 and Fig. S11). After 30 min, the DPPH• scavenging activity reached up to 76%. In opposition, lignins in solution scavenged at most 7% of DPPH• immediately after the assay start and 60% after 30 min. For comparison, Aadil et al. [56] reported DPPH radical scavenging capacity of different lignin fractions ranging from 50 to 94% after 20 min, while the antioxidant activity of ascorbic acid was reported as 28% at a concentration of 35 μg mL^{-1}.

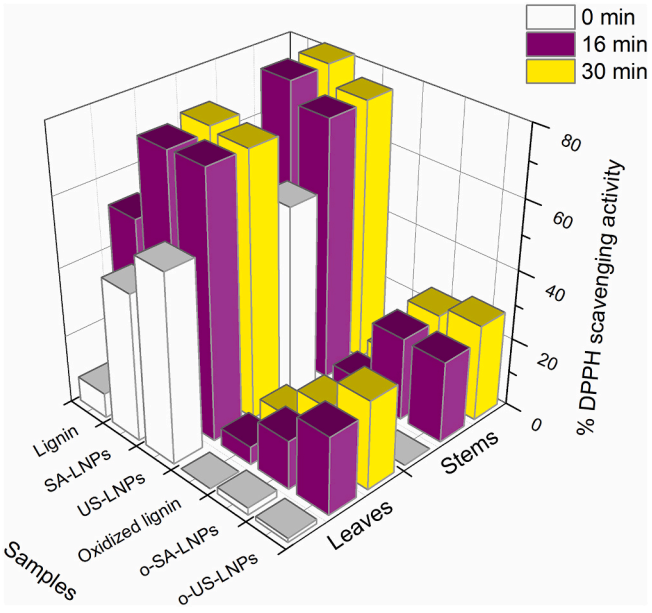

Fig. 9. DPPH radical scavenging activity measured for the samples of non-oxidized and oxidized lignin and LNPs from leaves and stems. Antioxidant capacity assay was performed for 0, 16, and 30 min.

Oxidation drastically reduced the antioxidant capacity of leaf and stem lignins in solution. The radical scavenging activity of oxidized lignins was up to eight times lower than that of their non-oxidized analogues. Although o-SA-LNPs and o-US-LNPs presented higher antioxidant activity than oxidized lignins in solution, this property was up to four times lower than that of non-oxidized LNPs. Kaur and co-workers [27] attributed this behavior to the reduction of the proportional amount of phenolic hydroxyl groups in lignin after oxidation.

Lignin capacity to scavenge free radicals is dependent on its ability to generate stable phenoxyl radicals. This property is compromised in oxidized lignin due to both the decreased concentration of phenolic groups and the presence of conjugated carbonyl groups that does not contribute to structure stabilization [27]. Self-assembly and ultrasonication/cavitation increased the specific surface area and the proportional exposition of hydroxyl and carboxyl groups onto entity surface, thus counterbalancing the oxidation effect and slightly improving the DPPH• scavenging activity of o-SA-LNPs and o-US-LNPs.

3.7. UV-photoabsorbance capability of lignin and oxidized lignin nanoparticles

As a model of the potential application of LNPs as additives in water-based nanocomposites, these nanoparticles were incorporated into a PVA matrix to form colored transparent films (Fig. 10A) with UV-absorption capacity. Usually, the content of LNPs added to transparent polymeric matrices is lower than 20% (*w/w*), so that the fixed concentration of 10% (*w/w*) studied here has been reported previously for targeted applications. Some examples include waterborne polyurethane nanocomposites [18], PVA nanocomposites with antioxidant and UV-protection abilities [57], cellulose nanocrystal/lignin UV-protection films [58] or cellulose nanofibril-based nanocomposites potentially suitable for food packaging, water purification, and biomedical products [59]. DRS analysis showed that the addition of 10% (*w/w*) non-oxidized or oxidized LNPs to the polymeric films increased their capability to photoabsorb in the ultraviolet/visible region (Fig. 10B, C). In addition to near zero transmittance at 200–300 nm, LNP-incorporated PVA films presented lower transmittance in the visible range than neat PVA.

SA-LNPs and US-LNPs from both leaves and stems imparted higher (though different) UV-absorption ability to PVA films than o-SA-LNPs and o-US-LNPs. Oxidized LNPs were less efficient for shielding in the UVA range (320–400 nm). Lignin possesses UV chromophore functional groups, including aromatic quinones and methoxy substituted phenoxy groups [60], which were likely altered during the prior oxidation process, as confirmed by the decreased extinction coefficient of the oxidized lignins.

Moreover, unsaturated functional groups such as conjugated carbonyl, aromatic rings, and C═C, which are also chromophores in the visible range [60], were prone to be degraded during oxidation. Hence, oxidation not only changed lignin brownish characteristic coloration, but also promoted reduction in lignin capability to absorb UV radiation.

4. Conclusions

An overview of this comprehensive study on lignin nanostructures is presented in Table 1, which compiles the main characteristics of self-assembled and ultrasonicated LNPs produced from oxidized or non-oxidized lignins extracted from elephant grass leaves or stems. The anatomical origin of starting lignin influenced the coloration of the yielded nanoparticles but did not significantly affect other properties besides the magnitude of zeta potentials.

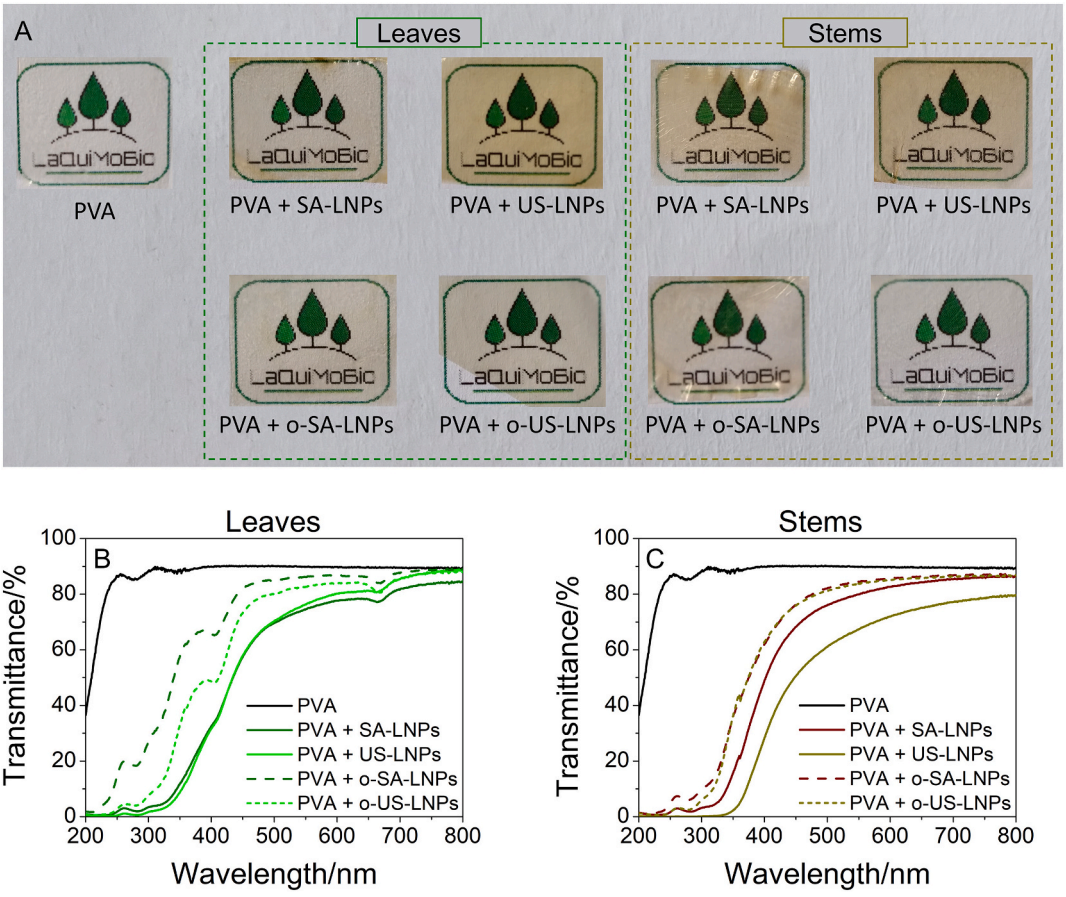

Fig. 10. (A) Photographs under visible light of self-standing neat PVA and PVA nanocomposite films incorporated with 10% (w/w) SA-LNPs, US-LNPs, o-SA-LNPs, or o-US-LNPs from leaf or stem lignin. (B, C) DRS spectra for neat PVA and PVA/LNP films.

Table 1
Overview of the main characteristics of nanolignins obtained from leaves and stems (diameter (D); content of ionizable groups (IG); zeta (ζ) potential at pH 7; antioxidant activity (AA) after 30-min DPPH• assay; absorbance at 280 nm (A_{280}) and at 500 nm (A_{500}) of LNP-containing PVA films).

	Nanolignin	D/nm	IG/mmol g^{-1}	ζ-potential/mV	AA/%	A_{280}/%	A_{500}/%
Leaves	SA-LNPs	50 ± 24	1.63 ± 0.18	−46 ± 6	78 ± 0,2	2	70
	o-SA-LNPs	21 ± 11	4.99 ± 0.44	−48 ± 4	17 ± 1	18	85
	US-LNPs	178 ± 91	1.87 ± 0.53	−41 ± 2	76 ± 1	0.6	70
	o-US-LNPs	170 ± 60	2.37 ± 0.18	−40 ± 1	26 ± 0,1	4	80
Stems	SA-LNPs	52 ± 28	1.60 ± 0.10	−39 ± 1	82 ± 0,5	2	76
	o-SA-LNPs	25 ± 8	4.69 ± 0.02	−34 ± 3	25 ± 0,2	6	82
	US-LNPs	228 ± 77	1.30 ± 0.10	−32 ± 2	76 ± 1	0	61
	o-US-LNPs	214 ± 105	2.62 ± 0.50	−45 ± 6	28 ± 1	3	81

Since native lignin is a highly cross-linked biomacromolecule, its removal from the cell wall implies the fragmentation of its complex structure, especially during the alkaline stage of the pretreatment. The factors that most affect the properties of LNPs thus correlate with the lignin extraction steps, the existence or absence of functionalization (oxidation), and the procedures involved in its conversion to the nanoscale.

Nanospheres were obtained by a bottom-up approach (addition of water as antisolvent) with higher yields than the globular/irregular aggregates produced by the top-down method (ultrasonication). Self-assembled LNPs were smaller and had more ionizable groups on the surface than ultrasonicated LNPs. Even though all LNPs showed higher charge density than the precursor bulk lignins, prior oxidation was crucial for obtaining nanoparticles with outstanding colloidal stability (very negative zeta potentials) and contents of ionizable groups, which include phenolic hydroxyls and carboxyls. Oxidation, however, also reduced LNP antioxidant activity and UV-blocking ability.

In conclusion, nanolignin properties can be tailored using different oxidation degrees of starting lignin, as well as distinct nanoparticle production methods. While the top-down approach presented here is beneficial as an organic solvent-free, 100% water-based protocol which allows for eliminating energy-consuming drying steps, the bottom-up approach takes advantage of the intrinsic amphiphilic nature of lignin to produce nanoparticles with a more controlled morphology. Therefore, both methodologies could be strategic for generating value-added lignin nanoparticles intended for various end uses, including coatings, cosmetics, and polymer reinforcement.

CRediT authorship contribution statement

Camilla H. M. Camargos: Conceptualization, Data curation, Formal analysis, Investigation, Methodology, Validation, Visualization, Writing

- original draft, Writing - review & editing. **Camila A. Rezende:** Conceptualization, Funding acquisition, Project administration, Resources, Supervision, Writing - review & editing.

Declaration of competing interest

None.

Acknowledgements

We thank IQ-UNICAMP for providing infrastructure and access to analysis equipment, and Prof. Fernando Galembeck and Dr. Douglas Soares for providing access to the AFM facility. We acknowledge Prof. Eliana Duek and Priscila Breda (Biomaterial Laboratory, PUC-SP) for providing GPC analysis and access to the OM facility. Financial support was granted by São Paulo Research Foundation (FAPESP, grant 2018/23769-1), National Council for Scientific and Technological Development (CNPq, grants 140558/2017-9 and 420031/2018-9), and Coordenação de Aperfeiçoamento de Pessoal de Nível Superior – Brazil (CAPES, financial code 001).

Appendix A. Supplementary data

Supplementary data to this article can be found online at https://doi.org/10.1016/j.ijbiomac.2021.10.094.

References

[1] D. Kai, M.J. Tan, P.L. Chee, Y.K. Chua, Y.L. Yap, X.J. Loh, Towards lignin-based functional materials in a sustainable world, Green Chem. 18 (2016) 1175–1200, https://doi.org/10.1039/c5gc02616d.
[2] F. Cotana, G. Cavalaglio, A. Nicolini, M. Gelosia, V. Coccia, A. Petrozzi, L. Brinchi, Lignin as co-product of second generation bioethanol production from ligno-cellulosic biomass, in: Energy Procedia, Elsevier Ltd, 2014, pp. 52–60, https://doi.org/10.1016/j.egypro.2014.01.007.
[3] C.H.M. Camargos, R.A.P. Silva, Y. Csordas, L.L. Silva, C.A. Rezende, Experimentally designed corn biomass fractionation to obtain lignin nanoparticles and fermentable sugars, Ind. Crop. Prod. 140 (2019), 111649, https://doi.org/10.1016/j.indcrop.2019.111649.
[4] F. Zikeli, V. Vinciguerra, A. D'Annibale, D. Capitani, M. Romagnoli, G. S. Mugnozza, Preparation of lignin nanoparticles from wood waste for wood surface treatment, Nanomaterials. 9 (2019) 281, https://doi.org/10.3390/nano9020281.
[5] M. Österberg, M.H. Sipponen, B.D. Mattos, O.J. Rojas, Spherical lignin particles: a review on their sustainability and applications, Green Chem. 22 (2020) 2712–2733, https://doi.org/10.1039/d0gc00096e.
[6] H. Trevisan, C.A. Rezende, Pure, stable and highly antioxidant lignin nanoparticles from elephant grass, Ind. Crop. Prod. 145 (2020), 112105, https://doi.org/10.1016/j.indcrop.2020.112105.
[7] D. Tian, J. Hu, J. Bao, R.P. Chandra, J.N. Saddler, C. Lu, Lignin valorization: lignin nanoparticles as high-value bio-additive for multifunctional nanocomposites, Biotechnol. Biofuels. 10 (2017) 192, https://doi.org/10.1186/s13068-017-0876-z.
[8] A. Brandt, J. Gräsvik, J.P. Hallett, T. Welton, Deconstruction of lignocellulosic biomass with ionic liquids, Green Chem. 15 (2013) 550–583, https://doi.org/10.1039/c2gc36364j.
[9] W. Gao, P. Fatehi, Lignin for polymer and nanoparticle production: current status and challenges, Can. J. Chem. Eng. 97 (2019) 2827–2842, https://doi.org/10.1002/CJCE.23620.
[10] K. Minu, K.K. Jiby, V.V.N. Kishore, Isolation and purification of lignin and silica from the black liquor generated during the production of bioethanol from rice straw, Biomass Bioenergy 39 (2012) 210–217, https://doi.org/10.1016/J.BIOMBIOE.2012.01.007.
[11] A. García, A. Toledano, L. Serrano, I. Egüés, M. González, F. Marín, J. Labidi, Characterization of lignins obtained by selective precipitation, Sep. Purif. Technol. 68 (2009) 193–198, https://doi.org/10.1016/j.seppur.2009.05.001.
[12] P.K. Mishra, A. Ekielski, The self-assembly of lignin and its application in nanoparticle synthesis: a short review, Nanomaterials. 9 (2019), https://doi.org/10.3390/nano9020243.
[13] S. Iravani, R.S. Varma, Greener synthesis of lignin nanoparticles and their applications, Green Chem. 22 (2020) 612–636, https://doi.org/10.1039/c9gc02835h.
[14] S. Beisl, A. Miltner, A. Friedl, Lignin from micro- to nanosize: production methods, Int. J. Mol. Sci. 18 (2017) 1–30, https://doi.org/10.3390/ijms18061244.
[15] W.D.H. Schneider, A.J.P. Dillon, M. Camassola, Lignin nanoparticles enter the scene: a promising versatile green tool for multiple applications, Biotechnol. Adv. 47 (2021), 107685, https://doi.org/10.1016/j.biotechadv.2020.107685.
[16] F. Xiong, Y. Han, S. Wang, G. Li, T. Qin, Y. Chen, F. Chu, Preparation and formation mechanism of size-controlled lignin nanospheres by self-assembly, Ind. Crop. Prod. 100 (2017) 146–152, https://doi.org/10.1016/j.indcrop.2017.02.025.
[17] I.A. Gilca, V.I. Popa, C. Crestini, Obtaining lignin nanoparticles by sonication, Ultrason. Sonochem. 23 (2015) 369–375, https://doi.org/10.1016/j.ultsonch.2014.08.021.
[18] M.N.G. Gonzalez, M. Levi, S. Turri, G. Griffini, Lignin nanoparticles by ultrasonication and their incorporation in waterborne polymer nanocomposites, J. Appl. Polym. Sci. 134 (2017) 1–10, https://doi.org/10.1002/app.45318.
[19] S.S. Nair, S. Sharma, Y. Pu, Q. Sun, S. Pan, J.Y. Zhu, Y. Deng, A.J. Ragauskas, High shear homogenization of lignin to nanolignin and thermal stability of nanolignin-polyvinyl alcohol blends, ChemSusChem. 37996 (2014) 3513–3520, https://doi.org/10.1002/cssc.201402314.
[20] M.B. Agustin, P.A. Penttilä, M. Lahtinen, K.S. Mikkonen, Rapid and direct preparation of lignin nanoparticles from alkaline pulping liquor by mild ultrasonication, ACS Sustain. Chem. Eng. 7 (2019) 19925–19934, https://doi.org/10.1021/acssuschemeng.9b05445.
[21] M. Lievonen, J.J. Valle-Delgado, M.-L. Mattinen, E.-L. Hult, K. Lintinen, M. A. Kostiainen, A. Paananen, G.R. Szilvay, H. Setälä, M. Österberg, A simple process for lignin nanoparticle preparation, Green Chem. 18 (2016) 1416–1422, https://doi.org/10.1039/C5GC01436K.
[22] I.V. Pylypchuk, A. Riazanova, M.E. Lindström, O. Sevastyanova, Structural and molecular-weight-dependency in the formation of lignin nanoparticles from fractionated soft- and hardwood lignins, Green Chem. 23 (2021) 3061–3072, https://doi.org/10.1039/d0gc04058d.
[23] P. Figueiredo, C. Ferro, M. Kemell, Z. Liu, A. Kiriazis, K. Lintinen, H.F. Florindo, J. Yli-Kauhaluoma, J. Hirvonen, M.A. Kostiainen, H.A. Santos, Functionalization of carboxylated lignin nanoparticles for targeted and pH-responsive delivery of anticancer drugs, Nanomedicine 12 (2017) 2581–2596, https://doi.org/10.2217/nnm-2017-0219.
[24] M.L. Mattinen, J.J. Valle-Delgado, T. Leskinen, T. Anttila, G. Riviere, M. Sipponen, A. Paananen, K. Lintinen, M. Kostiainen, M. Österberg, Enzymatically and chemically oxidized lignin nanoparticles for biomaterial applications, Enzym. Microb. Technol. 111 (2018) 48–56, https://doi.org/10.1016/j.enzmictec.2018.01.005.
[25] A. Henn, M.L. Mattinen, Chemo-enzymatically prepared lignin nanoparticles for value-added applications, World J. Microbiol. Biotechnol. 35 (2019) 125–126, https://doi.org/10.1007/s11274-019-2697-7.
[26] A. Mancera, V. Fierro, A. Pizzi, S. Dumarçay, P. Gérardin, J. Velásquez, G. Quintana, A. Celzard, Physicochemical characterisation of sugar cane bagasse lignin oxidized by hydrogen peroxide, Polym. Degrad. Stab. 95 (2010) 470–476, https://doi.org/10.1016/j.polymdegradstab. 2010.01.012.
[27] R. Kaur, S.K. Uppal, Structural characterization and antioxidant activity of lignin from sugarcane bagasse, Colloid Polym. Sci. 293 (2015) 2585–2592, https://doi.org/10.1007/s00396-015-3653-1.
[28] W. He, W. Gao, P. Fatehi, Oxidation of Kraft lignin with hydrogen peroxide and its application as a dispersant for kaolin suspensions, ACS Sustain. Chem. Eng. 5 (2017) 10597–10605, https://doi.org/10.1021/acssuschemeng.7b02582.
[29] C.A. Rezende, B.W. Atta, M.C. Breitkreitz, R. Simister, L.D. Gomez, S.J. McQueen-Mason, Optimization of biomass pretreatments using fractional factorial experimental design, Biotechnol. Biofuels. 11 (2018) 206, https://doi.org/10.1186/s13068-018-1200-2.
[30] C.H.M. Camargos, C.A. Rezende, Structure-property relationships of cellulose nanocrystals and nanofibrils: implications for the design and performance of nanocomposites and all-nanocellulose systems, ACS Appl. Nano Mater. (2021), https://doi.org/10.1021/acsanm.1c02008.
[31] A.P. Richter, B. Bharti, H.B. Armstrong, J.S. Brown, D. Plemmons, V.N. Paunov, S. D. Stoyanov, O.D. Velev, Synthesis and characterization of biodegradable lignin nanoparticles with tunable surface properties, Langmuir 32 (2016) 6468–6477, https://doi.org/10.1021/acs.langmuir.6b01088.
[32] J.B. Sluiter, R.O. Ruiz, C.J. Scarlata, A.D. Sluiter, D.W. Templeton, Compositional analysis of lignocellulosic feedstocks. 1. Review and description of methods, J. Agric. Food Chem. 58 (2010) 9043–9053, https://doi.org/10.1021/jf1008023.
[33] A. Sluiter, B. Hames, R. Ruiz, C. Scarlata, J. Sluiter, D. Templeton, Determination of Sugars, Byproducts, and Degradation Products in Liquid Fraction Process Samples: Laboratory Analytical Procedure (LAP), Issue Date: 12/08/2006, 2006, www.nrel.gov. (Accessed 1 May 2021).
[34] C.A. Rezende, M.A. de Lima, P. Maziero, E.R. DeAzevedo, W. Garcia, I. Polikarpov, Chemical and morphological characterization of sugarcane bagasse submitted to a delignification process for enhanced enzymatic digestibility, Biotechnol. Biofuels. 4 (2011) 54, https://doi.org/10.1186/1754-6834-4-54.
[35] J. Sameni, S. Krigstin, M. Sain, Acetylation & lignin solubility, Bioresources 12 (2017) 1548–1565. https://ojs.cnr.ncsu.edu/index.php/BioRes/article/view/BioRes_12_1_1548_Sameni_Solubility_Lignin_Acetylated_Lignin_Organic_Solvents/5048.
[36] N. Lin, C. Bruzzese, A. Dufresne, TEMPO-oxidized nanocellulose participating as crosslinking aid for alginate-based sponges, ACS Appl. Mater. Interfaces 4 (2012) 4948–4959, https://doi.org/10.1021/am301325r.
[37] X. Pan, J.F. Kadla, K. Ehara, N. Gilkes, J.N. Saddler, Organosolv ethanol lignin from hybrid poplar as a radical scavenger: relationship between lignin structure, extraction conditions, and antioxidant activity, J. Agric. Food Chem. 54 (2006) 5806–5813, https://doi.org/10.1021/jf0605392.
[38] C.M. Noronha, S.M. de Carvalho, R.C. Lino, P.L.M. Barreto, Characterization of antioxidant methylcellulose film incorporated with α-tocopherol nanocapsules, Food Chem. 159 (2014) 529–535, https://doi.org/10.1016/J.FOODCHEM.2014.02.159.

[39] J. Huang, S. Fu, L. Gan, Lignin chemistry and applications, 2019, https://doi.org/10.1016/C2016-0-04708-3.
[40] A. Lähdetie, T. Liitiä, T. Tamminen, A. Jääskeläinen, Reflectance UV-vis and UV resonance Raman spectroscopy in characterization of Kraft pulps, Bioresources 4 (2009) 1600–1619. https://ojs.cnr.ncsu.edu/index.php/BioRes/article/viewFile/BioRes_04_4_1600_Lahdetie_LTJ_Reflec_UV_Vis_Raman_Spec_kraft_pulps/464.
[41] H. Sun, L. Biedermann, T.C. Bond, Color of brown carbon: a model for ultraviolet and visible light absorption by organic carbon aerosol, Geophys. Res. Lett. 34 (2007) L17813, https://doi.org/10.1029/2007GL029797.
[42] J. Laskin, A. Laskin, S.A. Nizkorodov, P. Roach, P. Eckert, M.K. Gilles, B. Wang, H. J. Lee, Q. Hu, Molecular selectivity of brown carbon chromophores, Environ. Sci. Technol. 48 (2014) 12047–12055, https://doi.org/10.1021/es503432r.
[43] R. Sun, J. Tomkinson, F.C. Mao, X.F. Sun, Physicochemical characterization of lignins from rice straw by hydrogen peroxide treatment, J. Appl. Polym. Sci. 79 (2001) 719–732, https://doi.org/10.1002/1097-4628(20010124)79:4<719::AID-APP170>3.0.CO;2-3.
[44] F.C. Moreira-Vilar, S.-S. Rdc, A. Finger-Teixeira, O. Dmd, A.P. Ferro, The acetyl bromide method is faster, simpler and presents best recovery of lignin in different herbaceous tissues than klason and thioglycolic acid methods, PLoS One. 9 (2014), 110000, https://doi.org/10.1371/journal.pone.0110000.
[45] M.R.C. Fernandes, X. Huang, H.C.L. Abbenhuis, E.J.M. Hensen, Lignin oxidation with an organic peroxide and subsequent aromatic ring opening, Int. J. Biol. Macromol. 123 (2019) 1044–1051, https://doi.org/10.1016/j.ijbiomac.2018.11.105.
[46] F. Xu, J. Yu, T. Tesso, F. Dowell, D. Wang, Qualitative and quantitative analysis of lignocellulosic biomass using infrared techniques : a mini review, Appl. Energy 104 (2013) 801–809, https://doi.org/10.1016/j.apenergy.2012.12.019.
[47] C.M. Popescu, M.C. Popescu, G. Singurel, C. Vasile, D.S. Argyropoulos, S. Willfor, Spectral characterization of eucalyptus wood, Appl. Spectrosc. 61 (2007) 1168–1177, https://doi.org/10.1366/000370207782597076.
[48] D.L. Pavia, G.M. Lampman, G.S. Kriz, Introduction to Spectroscopy, Third Ed., CENGAGE Learning, 2015 https://doi.org/10.1201/9781439894651-21.
[49] H. Li, Y. Deng, J. Liang, Y. Dai, B. Liu, Y. Ren, X. Qiu, C. Li, Direct preparation of hollow nanospheres with Kraft lignin: a facile strategy for effective utilization of biomass waste, Bioresources 11 (2016) 3073–3083, https://doi.org/10.15376/biores.11.2.3073-3083.
[50] J.Y. Zhu, U.P. Agarwal, P.N. Ciesielski, M.E. Himmel, R. Gao, Y. Deng, M. Morits, M. Österberg, Towards sustainable production and utilization of plant-biomass-based nanomaterials: a review and analysis of recent developments, Biotechnol. Biofuels. 14 (2021) 1–31, https://doi.org/10.1186/s13068-021-01963-5.
[51] T. Seino, A. Yoshioka, M. Fujiwara, K.L. Chen, T. Erata, M. Tabata, M. Takai, ESR studies of radicals generated by ultrasonic irradiation of lignin solution. An application of the spin trapping method, Wood Sci. Technol. 35 (2001) 97–106, https://doi.org/10.1007/s002260000080.
[52] P.C. Hiemenz, R. Rajagopalan, in: Principles of Colloid and Surface Chemistry, 10.1016/0021-9797(79)90045-6, 1997, p. 650, https://doi.org/10.1016/0021-9797(79)90045-6.
[53] M. Österberg, M.H. Sipponen, B.D. Mattos, O.J. Rojas, Spherical lignin particles: a review on their sustainability and applications, Green Chem. 22 (2020) 2712–2733, https://doi.org/10.1039/d0gc00096e.
[54] A. Duval, M. Lawoko, A review on lignin-based polymeric, micro- and nano-structured materials, React. Funct. Polym. 85 (2014) 78–96, https://doi.org/10.1016/j.reactfunctpolym.2014.09.017.
[55] D. Tian, J. Hu, R.P. Chandra, J.N. Saddler, C. Lu, Valorizing recalcitrant cellulolytic enzyme lignin via lignin nanoparticles fabrication in an integrated biorefinery, ACS Sustain. Chem. Eng. 5 (2017) 2702–2710, https://doi.org/10.1021/acssuschemeng.6b03043.
[56] K.R. Aadil, A. Barapatre, S. Sahu, H. Jha, B.N. Tiwary, Free radical scavenging activity and reducing power of Acacia nilotica wood lignin, Int. J. Biol. Macromol. 67 (2014) 220–227, https://doi.org/10.1016/J.IJBIOMAC.2014.03.040.
[57] X. He, F. Luzi, X. Hao, W. Yang, L. Torre, Z. Xiao, Y. Xie, D. Puglia, Thermal, antioxidant and swelling behaviour of transparent polyvinyl (alcohol) films in presence of hydrophobic citric acid-modified lignin nanoparticles, Int. J. Biol. Macromol. 127 (2019) 665–676, https://doi.org/10.1016/j.ijbiomac.2019.01.202.
[58] M. Parit, P. Saha, V.A. Davis, Z. Jiang, Transparent and homogenous cellulose nanocrystal/lignin UV-protection films, ACS Omega 3 (2018) 10679–10691, https://doi.org/10.1021/acsomega.8b01345.
[59] M. Farooq, T. Zou, G. Riviere, M.H. Sipponen, M. Österberg, Strong, ductile, and waterproof cellulose nanofibril composite films with colloidal lignin particles, Biomacromolecules 20 (2019) 693–704, https://doi.org/10.1021/acs.biomac.8b01364.
[60] H. Sadeghifar, A. Ragauskas, Lignin as a UV light blocker-a review, Polymers (Basel). 12 (2020) 1–10, https://doi.org/10.3390/POLYM12051134.